HAL open science

Assessment of the mechanical errors of a prototype of an optical multilateration system

J. Guillory, D. Truong, J.-P. Wallerand

▶ **To cite this version:**

J. Guillory, D. Truong, J.-P. Wallerand. Assessment of the mechanical errors of a prototype of an optical multilateration system. Review of Scientific Instruments, 2020, 91 (2), pp.025004. 10.1063/1.5132933 . hal-03723954

HAL Id: hal-03723954

https://cnam.hal.science/hal-03723954v1

Submitted on 15 Jul 2022

HAL is a multi-disciplinary open access archive for the deposit and dissemination of scientific research documents, whether they are published or not. The documents may come from teaching and research institutions in France or abroad, or from public or private research centers.

L'archive ouverte pluridisciplinaire **HAL**, est destinée au dépôt et à la diffusion de documents scientifiques de niveau recherche, publiés ou non, émanant des établissements d'enseignement et de recherche français ou étrangers, des laboratoires publics ou privés.

Distributed under a Creative Commons Attribution 4.0 International License

Review of Scientific Instruments

Assessment of the mechanical errors of a prototype of an optical multilateration system

Cite as: Rev. Sci. Instrum. **91**, 025004 (2020); https://doi.org/10.1063/1.5132933
Submitted: 21 October 2019 • Accepted: 30 January 2020 • Published Online: 18 February 2020

J. Guillory, D. Truong and J.-P. Wallerand

View Online Export Citation CrossMark

ARTICLES YOU MAY BE INTERESTED IN

SI-traceable absolute distance measurement over more than 800 meters with sub-nanometer interferometry by two-color inline refractivity compensation
Applied Physics Letters **111**, 191104 (2017); https://doi.org/10.1063/1.5000569

Stability investigation of a cryo soft x-ray microscope by fiber interferometry
Review of Scientific Instruments **91**, 023701 (2020); https://doi.org/10.1063/1.5138369

Review of Scientific Instruments New Products
Review of Scientific Instruments **91**, 029501 (2020); https://doi.org/10.1063/5.0002748

Read Now!
Review of Scientific Instruments
Special Issue: Advances in Measurements and Instrumentation Leveraging Embedded Systems

© 2020 Author(s).

Review of Scientific Instruments | ARTICLE | scitation.org/journal/rsi

Assessment of the mechanical errors of a prototype of an optical multilateration system

Cite as: Rev. Sci. Instrum. 91, 025004 (2020); doi: 10.1063/1.5132933
Submitted: 21 October 2019 • Accepted: 30 January 2020 •
Published Online: 18 February 2020

View Online Export Citation CrossMark

J. Guillory,[a] D. Truong, and J.-P. Wallerand

AFFILIATIONS

Conservatoire National des Arts et Métiers (Cnam), Laboratoire commun de métrologie LNE-Cnam, 1 rue Gaston Boissier, 75015 Paris, France

[a]Author to whom correspondence should be addressed: joffray.guillory@cnam.fr

ABSTRACT

We are developing a multilateration system at a reasonable cost that aims at an accuracy better than 50 μm determined with a consistent metrological approach. In this context, an absolute distance meter, developed in-house, is used as a unique telemetric system to feed the different measurement heads of the multilateration system through a network of optical fibers. The uncertainty contribution for a distance measurement of the telemetric system itself, in a controlled environment, is from 2 μm up to 100 m (k = 1). In this paper, the uncertainty contribution due to mechanical designs of the measurement heads and the target is estimated: the gimbal mechanisms we have designed are presented and their sources of error are identified, experimentally quantified, and minimized. At the end, we demonstrate that the current design of the measurement head does not induce errors higher than 2 μm on the measured distances and the design of the target does not induce errors higher than 9 μm.

© 2020 Author(s). All article content, except where otherwise noted, is licensed under a Creative Commons Attribution (CC BY) license (http://creativecommons.org/licenses/by/4.0/). https://doi.org/10.1063/1.5132933

I. INTRODUCTION

Large Volume Metrology (LVM)—means the ability to measure the size, location, orientation, and shape of large objects—is a critical requirement in many industries such as aerospace,[1] automotive,[2] and civil engineering where autonomous, reconfigurable, cost-effective, and/or highly productive precision manufacturing is required.[3,4] LVM is also used in surveying for alignment of large advanced science facilities such as those at CERN.[5]

Nowadays, commercial laser trackers are extensively used in these high value industries.[6] By measuring both the distance and the angle from the tracker to a reflector, thanks to a laser beam, a typical accuracy of 10 μm + 5 μm/m can be achieved.[7] These laser trackers with interferometric systems are highly performant for length measurements, but their accuracy is ultimately limited by the angle measurements.[8]

Therefore, the multilateration coordinate measurement technique appears as a good alternative since it eliminates the angular contribution, although it requires a large number of distance meters distributed throughout the space.[9] Indeed, the distances between four measuring stations and one target, associated with different target locations, provide sufficient information to establish the spatial locations of the target and that of the measuring heads themselves (using the self-calibration technique[10–13]). Such multilateration systems based on interferometry were already demonstrated and commercialized, using fringe counting interferometry with commercial laser tracer devices[14] or more recently using Frequency Scanning Interferometry.[15] However, to make multilateration more attractive, novel distance meters able to bridge the gap between expensive but accurate laser trackers (or tracers) and cheaper but less accurate devices [indoor Global Positioning System (GPS) and photogrammetric system] must emerge.[16]

To this end, we have developed an Absolute Distance Meter (ADM) based on the phase measurement of an amplitude-modulated light to use it in a multilateration system. ADMs are generally preferred in harsh environments as they provide a better flexibility of use and a greater robustness than interferometric displacement measurement systems. Indeed, they accept obstructions

© Author(s) 2020

of the beam path and important air turbulences contrary to the classical fringe counting interferometer systems. To reduce the global cost, the developed ADM is used as a unique telemetric system that feeds the different measurement heads of the multilateration system through a network of optical fibers. The cost of the telemetric system, principally the cost of the opto-electronic components, is thus shared between the motorized heads, which aim at a common reflector.

The objective is to realize a reference multilateration system at a reasonable cost with an accuracy better than 50 μm (coverage factor k = 1) determined with a consistent metrological approach. Such a system could be used, for instance, as a reference for on-site calibration of the indoor Global Positioning System (GPS)[17] or photogrammetric systems. Over distances of 10 m, indoor GPS has uncertainties in the range of 85–500 μm (k = 1) depending on the system configurations,[18] while dual camera photogrammetric systems claim uncertainties as low as 50 μm (k = 1).[19] The uncertainty contribution of the telemetric system itself has already been characterized in Ref. 20. A global uncertainty budget for the measurement of a mechanical displacement (distance between two positions of a same reflector) has been formally detailed, and an accuracy below 4 μm (k = 1) has been demonstrated for distances less than 1 km. This has been validated with displacement measurements up to 100 m, indoors, in a controlled environment: an uncertainty around 2 μm (k = 1) has been experimentally observed.

Now, we need to ensure that the mechanical designs of the measurement heads and that of the target will also contribute to accuracy by less than 50 μm for a distance measurement. In this paper, we will present how we can measure and minimize the mechanical errors of the gimbal mechanisms we have designed for rotation of measurement heads and the target. Section II briefly presents the shared ADM and the details about our multilateration system. Then, Sec. III focuses on the mechanical designs of the measurement heads and the target: the different mechanical sources of error are identified and modeled with appropriate parameters, and the errors induced on a distance measurement are presented in the form of equations. In Sec. IV, the mechanical parameters are measured using experimental procedures, and finally, an uncertainty budget on their effects on a distance measurement is detailed.

II. MULTILATERATION SYSTEM

In the multilateration system depicted in Fig. 1, a unique telemetric system (i.e., a shared ADM) feeds the different measurement heads, thanks to a network of singlemode fibers based on a 1 × 4 optical switch. Each head includes a collimating system and a motorized gimbal mechanism to aim at the target, a hollow corner cube. The target has also a motorized gimbal mechanism for automatic alignment with the heads when a distance measurement is required. The system is also compatible with commercial Spherically Mounted Retroreflectors (SMR).

In practice, the distance measurements are performed in a pure time-division multiplex: after alignment of the four measurement heads, the corner cube will turn alternately in the direction of each head, at the rate of the optical switch, to perform the four distance measurements. Such a choreography can be achieved in less than 20 s. It is then possible to move the target to another position. After at least nine target positions,[11,12] a multilateration algorithm can be applied for three-dimensional position determination from the set of distance measurements (4 × 9 distances).

The developed ADM uses the same operation principle as the one described in our previous publication:[20] the distance L traveled by a modulated light in air is determined by measuring the phase ϕ accumulated by the modulating Radio Frequency (RF) carrier during its propagation,

$$L = \frac{1}{2} \times \left(\frac{\phi}{2\pi} + k \right) \times \frac{c}{n \times f_{RF}}, \tag{1}$$

with c being the speed of light in vacuum, n the group refractive index of air, f_{RF} the modulation frequency, and k an integer number, called order, corresponding to the number of times that the phase of the amplitude modulation has rotated by 2π during the propagation.

In practice, the ADM is realized using telecommunication components that are reliable, largely available, and affordable. A 1550 nm optical carrier is emitted by a laser diode, intensity modulated using a RF carrier around 5 GHz, and amplified. This fiber-guided optical signal is then routed using the 1 × 4 optical switch to one measurement head where it is emitted in free space and collimated by an off-axis parabolic mirror (spot size of 9.2 mm at 1% power level). After propagating over several meters in air, the laser beam is

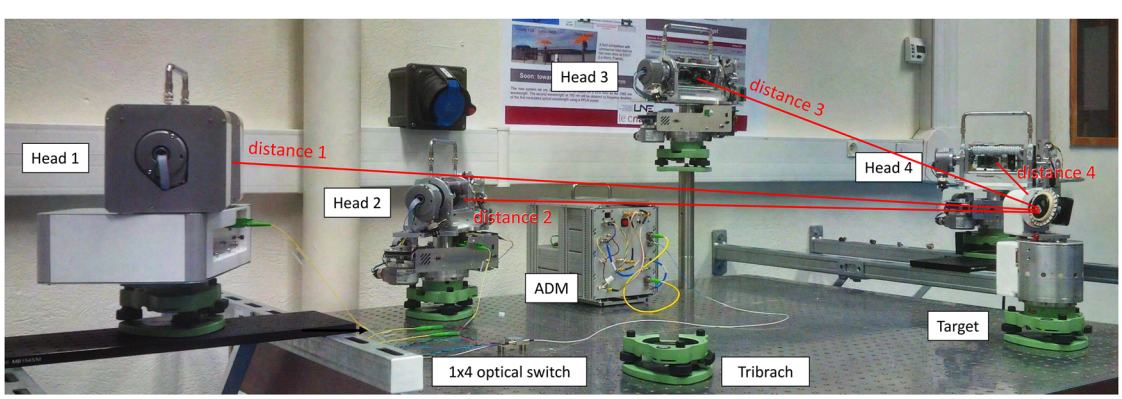

FIG. 1. Photograph of the developed multilateration system composed of a shared telemetric system, four measurement heads, and one target.

© Author(s) 2020

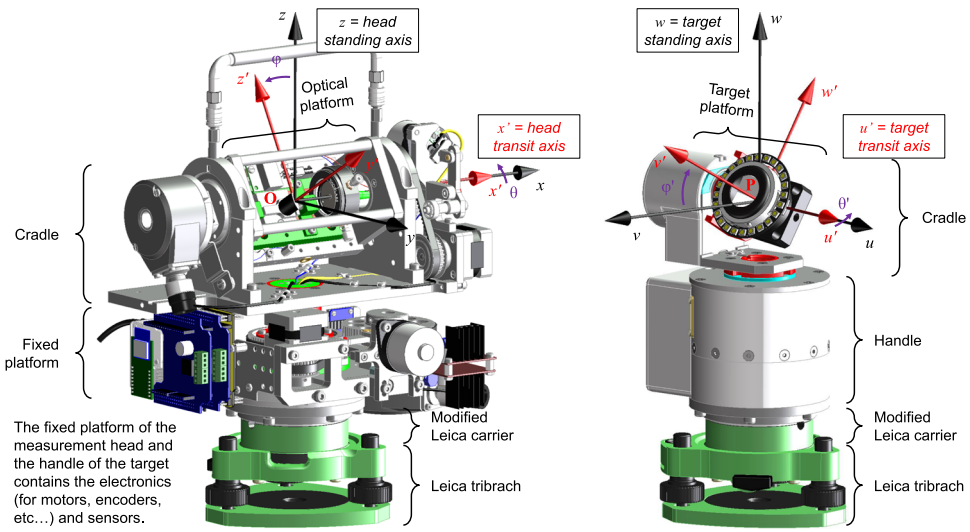

FIG. 2. 3D-view of the developed measurement heads and target for θ = θ′ = 0° and φ = φ′ = 30°.

reflected back toward the measurement head by the hollow corner cube and reinjected into the same singlemode fiber as previously. The returned signal is finally directed toward the telemetric system where a high-speed photodiode detects it and where the phase of the modulation RF carrier is measured.

Figure 2 depicts one of the four measurement heads we have developed. In an ideal system, the two rotating axes, called standing and transit, are orthogonal, and they intersect at a single point O from which the laser beam emerges. The platform for electronics and sensors is fixed, the cradle rotates around the standing axis only, and the optical platform rotates around the two axes. For rotation, stepping motors (400 steps per revolution) running in microstepping mode (16 microsteps per one full step) engage the rotation axes, thanks to a transmission belt with a factor of reduction of 32/72. Thus, they achieve an angular resolution of 436 μrad. The azimuth and elevation angles are recorded, thanks to angle encoders of 384 μrad of resolution, even if these values are not used for the determination of the three-dimensional positions of the target. Finally, the optical platform contains the optical collimating system, which is mounted on two translation stages that allow us to adjust the position of the origin of the optical laser beam.

The target, depicted on the right in Fig. 2, uses principles similar to the measurement head. Hence, the small platform that holds the corner cube up can be oriented in any direction. Its compact design, with electronics running on battery, permits one-hand operation to move the target from one position to another. The target does not have angle encoders, but it is equipped with optical forked sensors that define set points for the zero adjustment of the angles.

In Sec. III, the different sources of errors of these gimbal mechanisms are identified and modeled, and then, in Sec. IV, the parameters of these errors are measured for one of the four developed measurement heads and for the target.

III. MODELING OF THE ERRORS DUE TO GEOMETRIC MISALIGNMENTS

In order to define, in the most comprehensible way, the different sources of error in distance measurement due to the beam steering mechanism, we will use different orthogonal Cartesian systems (Fig. 2).

First, the x, y, and z axes form a fixed orthogonal Cartesian system with the point O as origin. The z axis is aligned on the standing axis of the measurement head, and the x axis is aligned with the transit axis when the azimuth angle (provided by the angle encoder) is equal to zero. By analogy, P uvw is a fixed orthogonal Cartesian system for the target.

Then, O x′y′z′ forms a third orthogonal Cartesian system attached to the optical platform of the head. This means that the x′ axis stays parallel to the transit axis, i.e., it rotates with the azimuth of the head, and the z′ axis turns with the elevation of the gimbal mechanism. By analogy, P u′v′w′ forms a last orthogonal Cartesian system attached to the platform of the corner cube.

A. Measurement head: Beam offset

The laser beam that should ideally pass by the intersection of the two rotation axes of the head, at the point O in Fig. 3, may be displaced from its ideal position by a constant offset. The error induced on the measured distance—defined as the difference between the true value (called Rt, for a true range) and the measured one (called Ri, for an intermediate range)—can be easily calculated using the following equation:

$$Rt^2 = Ri^2 + a^2 + c^2, \tag{2}$$

with a and c being the projections of the beam offset on the x′ and z′ axes, respectively. Explanation of formula (2) is given in Fig. 3 for a two-dimensional case.

B. Measurement head: Beam tilt

As depicted in Fig. 4, the laser beam, in addition to a beam offset error, may also be tilted from its ideal path, i.e., it may not be normal to the plane formed by the two axes x′ and z′. In that case, the beam path Ri changes to take into account the beam tilt, and formula (2) becomes more complex,

$$Rt^2 = Ri^2 + a^2 + c^2 - 2\,a\,Ri^*\sin(\alpha) - 2\,c\,Ri\sin(\gamma), \tag{3}$$

© Author(s) 2020

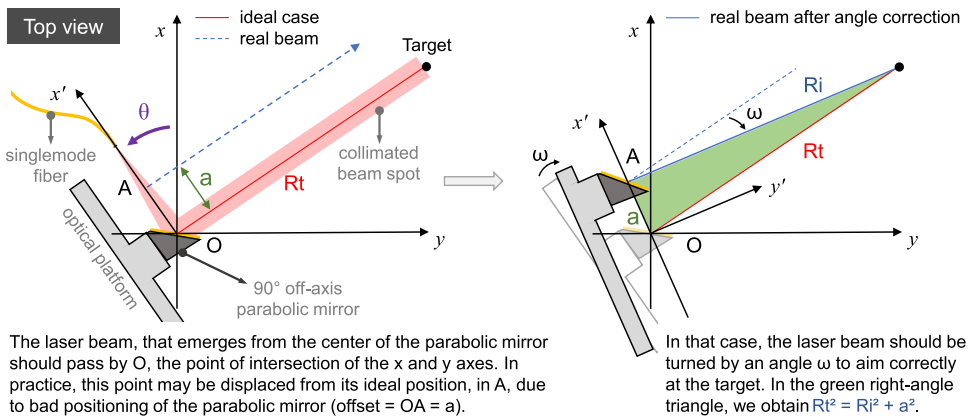

The laser beam, that emerges from the center of the parabolic mirror should pass by O, the point of intersection of the x and y axes. In practice, this point may be displaced from its ideal position, in A, due to bad positioning of the parabolic mirror (offset = OA = a).

In that case, the laser beam should be turned by an angle ω to aim correctly at the target. In the green right-angle triangle, we obtain $Rt^2 = Ri^2 + a^2$.

FIG. 3. Top view of the measurement head that reveals the beam offset error along the x′ axis. This view is a projection in the plane (xOy), i.e., z = 0.

with α and γ being the tilt angles formed with the y′ axis in the planes (x′Oy′) and (z′Oy′), respectively, and Ri* a value that can be approximated by Ri for a small beam offset along the z′ axis,

$$Ri^* = \mathrm{sqrt}(Ri^2 + c^2 - 2\,c\,Ri\sin(\gamma)). \tag{4}$$

It must be noted that beam tilt without beam offset does not induce an error on the distance measurements.

C. Measurement head: Transit offset

Finally, as depicted in Fig. 5, the transit axis may not intersect the standing axis due to an offset Toh from its ideal location. This offset, defined in the direction of y′ when the elevation angle is null (φ = 0), modifies the intermediate result Ri in formulas (3) and (4) as follows:

$$Rm^2 = Toh^2 + Ri^2 + 2\,Toh\,Ri^*\cos(\alpha) - \cos(\varphi - \gamma), \tag{5}$$

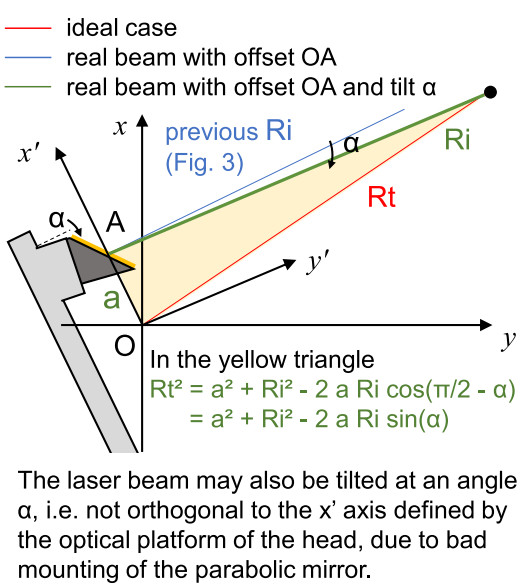

FIG. 4. Top view of the measurement head that reveals the beam tilt error along the x′ axis added to a beam offset.

with Rm being the experimentally measured value, Toh the transit offset, i.e., the distance between the standing and transit axes, φ the elevation angle of the gimbal mechanism, and α and γ the tilt angles formed with the y′ axis. The second-degree equation in formula (5) with Ri as the unknown parameter and Rm as variable has to be solved, and then, the result Ri has to be used in formulas (3) and (4) to find the true value Rt.

Of course, to aim correctly at the target, the azimuth and elevation angles should be slightly adjusted due to the transit offset (i.e., after displacement from O to O′). This is not taken into account above unless the provided formulas are good approximations, particularly if the beam tilt α is negligible (top view) and if the beam offset c is also negligible (side view).

D. Target: Offset

The corner cube should also be placed at the intersection of the two rotation axes of its gimbal mechanism, at the point P. If it is displaced from this ideal position by a constant offset, this induces an error on the measured distance. This error depends on the offsets in the three Cartesian directions, a′, b′, and c′, respectively, but also on the corner cube alignment defined by the azimuth angle θ′ and the elevation angle φ′. In practice, the perfect alignment with the measurement head is not always achieved: it must be better than the corner cube aperture, i.e., 30°. The small misalignment angles are noted θ″ and φ″.

Thus, in the local orthogonal Cartesian system P u′v′w′ attached to the corner cube, the error due to the target offsets, defined as the difference between the true value Rt and the measured one Ri, can be calculated from

$$Ri^2 = Rt^2 + a'^2 + 2\,Rt\,a'\sin(\theta'') + b'^2 - 2\,Rt\,b'\cos(\theta'')\cos(\varphi'') + c'^2 + 2\,Rt\,c'\sin(\varphi''). \tag{6}$$

Explanation of formula (6) is given in Fig. 6 for a two-dimensional case.

E. Target: Transit offset

As depicted in Fig. 7, the transit axis may not intersect the standing axis due to an offset Tot from its ideal location. This offset, defined in the direction of v′ when the elevation angle is null

© Author(s) 2020

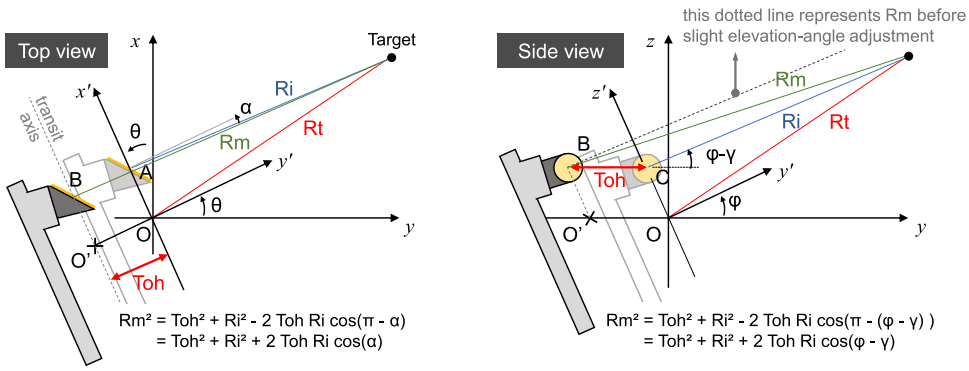

FIG. 5. Top view on the left and side view on the right reveal the transit offset error (Toh is, here, negative). The standing axis is still passing by the point O, but the transit axis is now passing by the point O′.

($\varphi' = 0$), can be interpreted as a new offset that depends on this elevation angle. Hence, in formula (6), the variables a', b', and c' are replaced by

$$\begin{aligned} a' &\to a' + 0, \\ b' &\to b' + \mathrm{Tot}\cos(\varphi'), \\ c' &\to c' - \mathrm{Tot}\sin(\varphi'), \end{aligned} \tag{7}$$

with Tot being the transit offset of the target, i.e., the distance between the standing and transit axes, and φ' the elevation angle of the gimbal mechanism. Previously, the error due to the transit offset of the target is limited by the corner cube aperture, and indeed, the θ' and φ' angles are included between $-15°$ and $+15°$.

After the use of formula (7) in formula (6), we obtain

$$\mathrm{Rm}^2 = \mathrm{Rt}^2 + \mathrm{Tot}^2 + a'^2 + b'^2 + c'^2 + 2g(\theta'', \varphi'', \varphi'), \tag{8}$$

with $g(\theta'', \varphi'', \varphi)$ being a function that describes the variations of Rm^2 as a function of the viewing angles. This function, null for $\theta'' = \varphi'' = \varphi' = 0$, is equal to

$$\begin{aligned} g(\theta'', \varphi'', \varphi') = {} & a'\,\mathrm{Rt}\sin(\theta'') + b'\,[\mathrm{Tot}\cos(\varphi') - \mathrm{Rt}\cos(\theta'')\cos(\varphi'')] \\ & + c'[\mathrm{Rt}\sin(\varphi') - \mathrm{Tot}\sin(\varphi')] \\ & - \mathrm{Tot}\,\mathrm{Rt}[\cos(\varphi')\cos(\theta'')\cos(\varphi'') \\ & + \sin(\varphi')\sin(\varphi'')]. \end{aligned} \tag{9}$$

F. Instrument distance offset

So far, the point O, the ideal point of the rotating axes intersection, has been considered as the point from which the laser beam

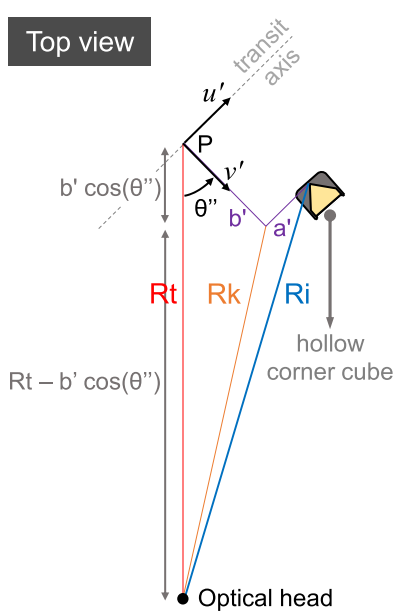

FIG. 6. Top view of the corner cube that highlights the target offset error in the plane (u′Pv′), i.e., w′ = 0.

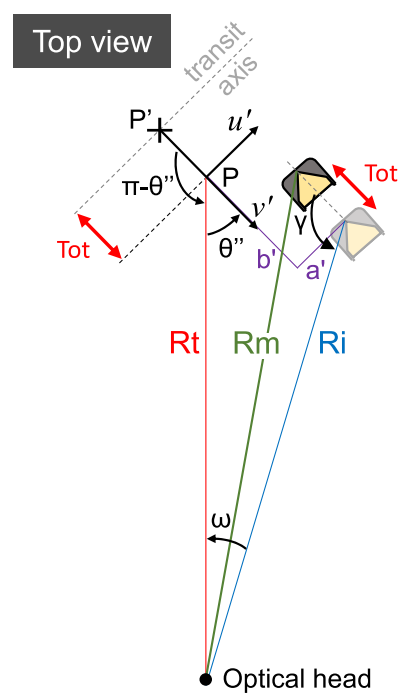

FIG. 7. Top view of the corner cube that highlights the target transit offset error. This is a projection in the plane (u′Pv′), i.e., w′ = 0.

© Author(s) 2020

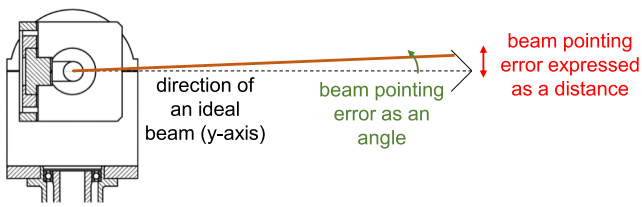

FIG. 8. Side view of the measurement head that highlights the pointing error.

emerges, i.e., from which the distance measurement is done. In practice, this point corresponds to the center of the parabolic mirror. By construction, the laser beam passes through this point, but a constant distance offset has to be considered for all the optical paths located upstream: this is the instrument offset.

On the side of the target, there is no distance offset. Nevertheless, we can adopt another approach and decide that the target offset along the u′ axes, i.e., b′ in Sec. III D, should be part of the instrument distance offset. This second option is more pragmatic if a good alignment between the measurement head and the target is ensured, i.e., θ′ and φ′ are equal to zero, which is not the case here.

The instrument offset can have a large impact on the error of the measured distance. However, for multilateration application, its value does not need to be known since it can be determined online using an algorithm with self-calibration.[11,12]

G. Pointing error

The ability of our system to aim correctly at the center of the corner cube is generally expressed as an angle value, ω_p, but it can also be expressed as a distance error, Pe (Fig. 8). These parameters do not induce errors on the distance measurements as the target is a hollow corner cube. However, a bad pointing can reduce the received power of the telemetric signal and can therefore introduce, indirectly, errors on the measured distance, for instance, due to crosstalk in the telemetric signal[20] (i.e., the addition of a spurious signal to the ideal measurement signal that induces a cyclic error, sinusoidal with the distance).

Finally, the pointing should not be considered as a source of mechanical error like any others. This mechanical limitation has an impact on the power received by the telemetric system, which is intrinsically linked to the signal-to-crosstalk ratio and so to the level of uncertainty. The mechanical design is therefore inherent to the whole system and it cannot be only studied as an isolated sub-system.

IV. ESTIMATION OF THE GEOMETRIC ERRORS

A. Measurement of the geometric errors of the measurement head

To measure the parameters of the misalignment of the gimbal mechanism of the measurement head, a double-centering method has been achieved (also called the double-face measurement). This method consists in pointing the same object under two different orientations of the head, thanks to a first rotation of 180° around the standing axis and then a second 180° rotation around the transit axis. Thus, the measurement head moves from the position θ = φ = 0 to the position θ = φ = π. In order to have an optical beam that points the same object after double-centering, the optical beam must emerge from the intersection of the two rotating axes, orthogonally to the plane formed by these axes, i.e., without beam offset, beam tilt, and transit offset. Otherwise, as depicted in Fig. 9, this procedure produces two measurements with opposite errors. That is precisely what we use to determine the error contributions of the measurement head.

In Fig. 10, the displacements of the beam spot Δx and Δz for different distances after double-centering have been plotted for two successive tests. In practice, the following procedure has been applied: first, the beam spot was centered on the corner cube; then, a double-centering was carried out; and, finally, the corner cube was moved using micrometric screws (by Δx and Δz) to be centered at the new beam spot position (i.e., perfect alignment). The centering of the corner cube on the laser beam is done by optimizing the telemetric signal. By this way, we can determine the beam spot displacements along the x and z axes with the uncertainty of the pointing.

The beam offsets (a and c) and the beam tilts (α and γ) can be determined from these measurements using the least squares method: the slope of a regression line corresponds to twice the tangent of the tilt angle, and its value at the distance zero corresponds to twice that of the beam offset. The least square method also provides standard deviations on the slope and on the intercept of the regression line:[21] with three experimental points, we typically get the angles with a standard deviation of 0.005° and the offsets with a standard deviation of 60 μm. Finally, the half distance difference between one distance measurement before and one distance measurement after double-centering gives a good approximation of the transit offset (for negligible beam offsets and tilts as in our case).

After a first measurement (test 1 in Fig. 10), the transit offset has been minimized by adjusting the position of the cradle (see Fig. 2). This parameter can be minimized down to 3 μm. Then, the beam offsets have been minimized, thanks to translation stages mounted on the head, enabling adjustment of the parabolic mirror position. Finally, the initial value of the elevation angle has been chosen so that the corresponding beam tilt is minimized. This cannot be done for the azimuth angle since the two rotation axes of the gimbal mechanism are not totally independent: a rotation around the standing axis lead to a rotation of the transit axis, but the reverse is false. After these adjustments, the following values for mechanical parameters with their uncertainty were measured (test 2 in Fig. 10):

$$a = 1.5\,\mu m \pm 60\,\mu m, c = -10.6\,\mu m \pm 60\,\mu m, \alpha = 0.171^\circ \pm 0.005^\circ,$$
$$\gamma = 0.017^\circ \pm 0.005^\circ, \text{ and } Toh = 3\mu m \pm 2\,\mu m.$$

Finally, the numerical application of formula (3) with these values shows that the beam offsets and the beam tilts have negligible effects as they induce an error on the measured distance lower than 250 nm (taking into account measurement uncertainty of these parameters). The only non-negligible error comes from the transit offset of 3 μm ± 2 μm (k = 1). As we know the elevation angle, thanks to the angle encoders, the measured distance can be corrected from this error with formula (5).

© Author(s) 2020

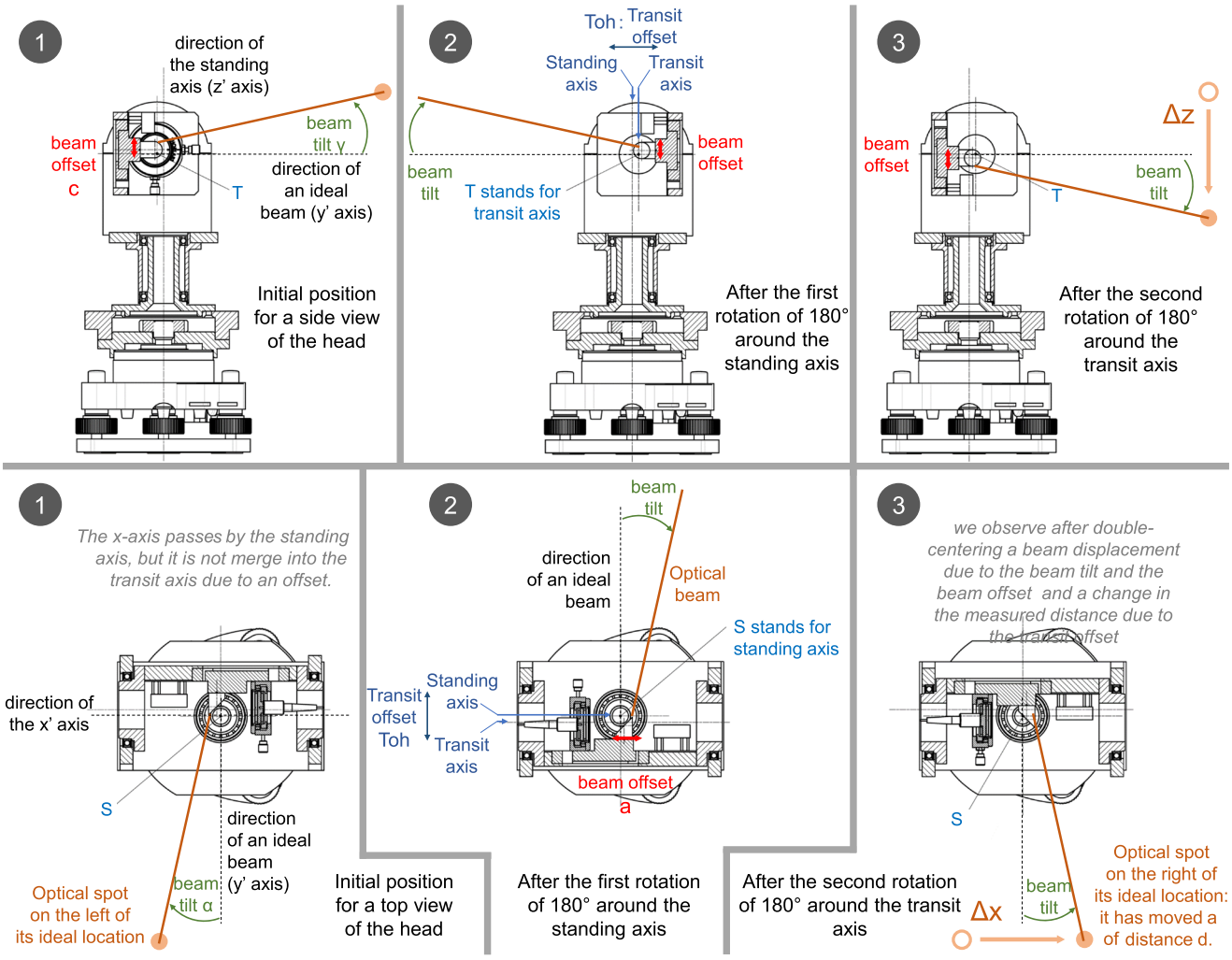

FIG. 9. Beam spot displacement due to a double-centering in three steps: side view of the head at the top of the picture (measurement of Δz and γ) and top view at the bottom (measurement of Δx and α).

B. Characterization of the target

In the same manner as the characterization of the measurement head, a good approximation of the transit offset (for negligible target offsets) is obtained by the half distance difference between one measurement before and one measurement after double-centering of the target. Thus, the latter has been estimated to be 11 μm ± 2 μm (k = 1).

There is no simple way to measure directly the offset parameters of the target, a', b', and c'. Therefore, in the first time, only measurements of the variations of the error induced on a distance of 57 cm as a function of the viewing angles have been performed. The results are presented in Table I.

The values obtained in Table I are particularly good with errors lower than 9 μm. Actually, the position of the corner cube has been mechanically adjusted after first measurements: initially, the variations were of the order of several hundreds of micrometers.

In a second time, from the theoretical model of Rm defined in formulas (8) and (9) and the values of Table I, we have minimized the quadratic sum of the vector,

$$[\mathrm{Rm}(\theta'',\varphi'') - \mathrm{Rm}(0,0)] - \text{Variations of Table I}(\theta'',\varphi''),$$
$$\text{with } \theta'' = [-15^\circ, 0^\circ, 15^\circ] \text{ and } \varphi'' = [-15^\circ, 0^\circ, 15^\circ],$$

using the Nelder–Mead method under Matlab. This consists in choosing the best values of a', b', and c' in $\mathrm{Rm}(\theta'', \varphi'')$ in order to obtain the same data between the theoretical model and the experimental results. In practice, this numerical method provides the following values:

$$a' = -6\,\mu\mathrm{m}, b' = 34\,\mu\mathrm{m}, \text{ and } c' = -22\,\mu\mathrm{m}.$$

Using these parameters, the differences between the theoretical model and the experimental measurements in Table I are less than

© Author(s) 2020

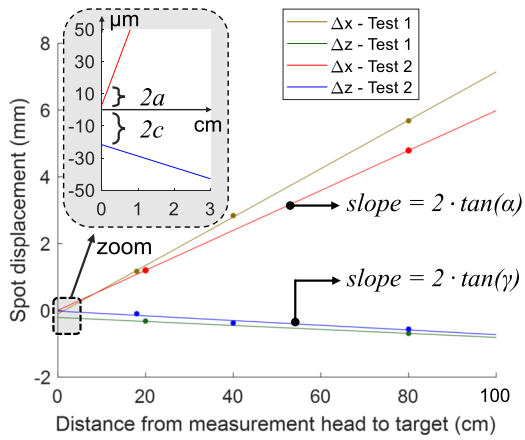

FIG. 10. Spot displacement after double-centering as a function of the distance.

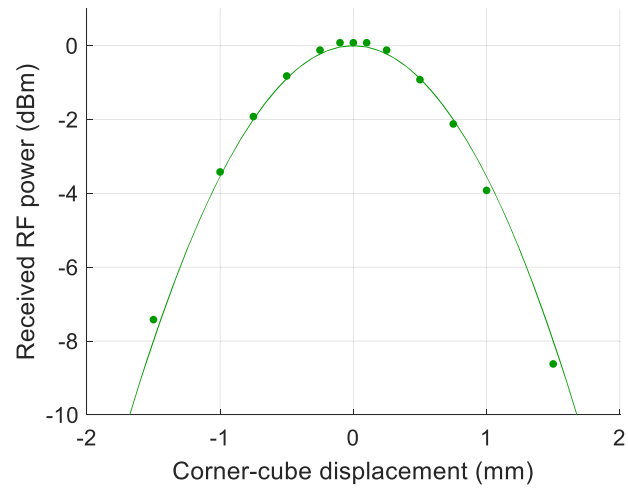

FIG. 11. Characterization of the pointing error. 1 dB power variation corresponds to 550 μm.

TABLE I. Variations of the distance Rm from the reference position $\theta' = \varphi' = 0$ for Rt = 57 cm as a function of the corner cube alignment.

		Elevation φ''		
		−15°	0°	+15°
Azimuth θ''	−15°	9 μm	3 μm	−1 μm
	0°	5 μm	0 μm	−5 μm
	+15°	8 μm	0 μm	−6 μm

1.9 μm with a standard deviation of 1.0 μm. These values are consistent with the uncertainty of our experimental measurements, i.e., 2 μm (k = 1).

C. Characterization of the pointing

The determination of the center of the target using the measurement head is achieved by optimizing the received power of the telemetric signal. The performances of the pointing depend therefore on our capability to correctly discriminate the maximum of power: in Fig. 11, we have measured the RF power received at the ADM input as a function of the displacement of the corner cube, displacement normal to the optical beam, and performed, thanks to a translation stage with a micrometric screw. This displacement is equivalent to a misalignment of the optical beam from the center of the target. Indoors, with small air turbulences, 1 dB of power variation can be easily discriminated and corresponds to an error of 550 μm in the pointing (Pe).

The capability to aim properly at the target also depends on the angular resolution of the gimbal mechanism. The latter, mainly limited by the stepper motors, is equal to 436 μrad (ωp).

With the use of a corner cube as retroreflector, no error is induced on the measured distance due to the pointing. However, with a motor resolution of 436 μrad, we can adjust the position of the beam spot with a resolution of 1.7 mm at 4 m, which can induce 10 dB of RF attenuation at the input of the telemetric system, i.e., the limit value to guarantee a correct measurement. As explained in Subsection III G, with the use of a corner cube as retroreflector, no error is induced on the measured distance due to the pointing. However, a bad pointing can reduce the received power of the telemetric signal and can therefore introduce, indirectly, errors on the measured distance due to crosstalk in the telemetric signal.[20] With a motor resolution of 436 μrad, we can adjust the position of the beam spot with a resolution of 1.7 mm at 4 m. Such a deviation can induce 10 dB of additional RF attenuation at the input of the telemetric system: this will reduce the signal to crosstalk ratio from 75 dB to 65 dB, and thus increase the uncertainty component due to crosstalk from 0.6 μm to 1.9 μm in the performance assessment of the telemetric system.

D. Summary and discussion

The different sources of error of the measurement heads and that of the target have been identified and modeled, and then, these errors have been quantified. Table II summarizes these errors due to geometric misalignments.

The gimbal mechanism of the measurement head we have characterized induces very low errors on the measured distances, especially if we correct the error due to the transit offset. Indeed, when the errors have been modeled and when their values are known, a correction can be done. In our case, by considering negligible beam offset and beam tilt, Formula (5) can be simplified as follows for correction:

$$\mathrm{Rm}^2 \approx \mathrm{Toh}^2 + \mathrm{Rt}^2 + 2\,\mathrm{Toh}\,\mathrm{Rt}\cos(\varphi), \tag{10}$$

with Rt being the true value, Rm the measured one, Toh the transit offset, and φ the elevation angle of the gimbal mechanism of the head. Rm and Toh are known, thanks to the developed ADM with an accuracy of 2 μm (k = 1), whereas the elevation angle is measured using the angle encoder at an accuracy better than 400 μrad.

At the end, the mechanical errors of the target are the most important components of the uncertainty budget: errors up to 9 μm are possible due to the target offset, and this cannot be corrected as

© Author(s) 2020

TABLE II. Uncertainty budget due to geometric misalignments.

i	Parameters	Description	Sources	Measured values	Error induced on the distance
1	a and c	Beam offset	Misalignment of the gimbal mechanism of the measurement head	1.5 μm and −10.6 μm ± 60 μm (k = 1)	Error <250 nm
2	α and γ	Beam tilt		0.171° and 0.017° ± 0.005° (k = 1)	
3	Toh	Transit offset of the head		3 μm ± 2 μm (k = 1)	<2 μm after Toh correction
4	a′, b′, and c′	Target offset	Misalignment of the gimbal mechanism of the target	−6 μm, 34 μm, and −22 μm	Error <9 μm
5	Tot	Transit offset of the target		11 μm ± 2 μm (k = 1)	<2 μm after Tot correction
6	Do	Distance offset (no impact for multilateration)	Difference between the measured distance and the mechanical one	Not measured	can be corrected
7	Pe and ω_P	Pointing error	Limited resolution of the pointing system	550 μm and 400 μrad	0 μm

the target is not equipped with angle encoders. The stepper motor drivers of the target are not sufficiently accurate for such a correction, but they can be used to determine which face of the corner cube is used ($\theta' = \varphi' = 0$ or $\theta' = \varphi' = \pi$) and thus remove partly the error due to the transit offset.

Concerning the instrument distance offset, its value has not been measured since its value does not need to be known for multilateration application (contrary to a simple distance measurement).

The system of aiming does not induce errors on the measured distance. However, this parameter is important as it highlights some limitations of the current motorized measurement heads: typically, beyond 4 m, the angular resolution of the stepper motors is not sufficient for accurate targeting. To resolve this, a fine tuning of the angles based on piezo motors is under development.

V. CONCLUSION

Our objective is to realize a reference multilateration system that proposes an accuracy better than 50 μm (k = 1) at a reasonable cost and with metrological traceability to SI meter. This system is composed of a telemetric system, four measurement heads, and a target. The uncertainty contribution of the telemetric system itself, based on the phase shift measurement of an intensity-modulated light, is around 2 μm (k = 1) for distances up to 100 m, which leaves us a considerable latitude for other sources of error.

In this paper, we have identified, modeled, and then quantified the different sources of error due to the motorized gimbal mechanisms of the measurement heads and the target for a multilateration system. The measurements of the parameters of these errors were realized by using double-centering procedures and for the target by using the comparison between experimental measurements and the theoretical model. Thus, the uncertainty budget for a distance measurement between one head and the target has been established. Through this, it has been shown that the current design of the measurement head does not induce errors higher than 2 μm. It is finally the gimbal mechanism of the target that represents the dominant source of uncertainty, with induced errors on the measured distance up to 9 μm.

The challenge to minimize the mechanical errors for different angular orientations of the heads and that of the rotating reflector appears to have been achieved. However, an evolution of the design of the heads is under development to add auxiliary motors and thus enable better angular resolutions for accurate targeting.

Finally, we should mention that the value of the air refractive index, which alters the propagation speed of the measuring beam, is a last source of uncertainty to take into account in such optical coordinate measurement systems. It depends on several atmospheric parameters,[22] but the most critical measurand in the air index determination is the temperature: it should be known with a precision of 1 °C along a 10 m optical path in order to determine the measured distance with an accuracy of 10 μm. To deal with this issue, acoustic thermometers are under development.

ACKNOWLEDGMENTS

This work was partially funded by Joint Research Projects (JRPs), 17IND03 LaVA and 18SIB01 GeoMetre, that have received funding from the European Metrology Programme for Innovation and Research (EMPIR) co-financed by the Participating States and from the European Union's Horizon 2020 research and innovation programme.

© Author(s) 2020

REFERENCES

[1] O. C. Martin, Z. Wang, P. Helgosson, J. E. Muelaner, A. Kayani, D. Tomlinson, and P. G. Maropoulos, "Metrology enhanced tooling for aerospace (META): A live fixturing, wing box assembly case study," in Proceedings of 7th International Conference on Digital Enterprise Technology (DET), Athens, Greece, 2011.

[2] E. Kiraci, P. Franciosa, G. A. Turley, A. Olifent, A. Attridge, and M. A. Williams, "Moving towards in-line metrology: Evaluation of a laser radar system for in-line dimensional inspection for automotive assembly systems," Int. J. Adv. Manuf. Technol. **91**(1-4), 69–78 (2017).

[3] M. R. Pedersenn, L. Nalpantidis, R. S. Andersen, C. Schou, S. Bøgh, V. Krüger, and O. Madsen, "Robot skills for manufacturing: From concept to industrial deployment," Rob. Comput. Integr. Manuf. **37**, 282–291 (2016).

[4] J. E. Muelaner and P. G. Maropoulos, "Large volume metrology technologies for the light controlled factory," in Proceedings of 8th International Conference on Digital Enterprise Technology (DET), Stuttgart, Germany, 2014.

[5] P. Arpaia, H. Mainaud Durand, and S. Russenschuck, "Editorial for the special feature on metrology for particle accelerators," Meas. Sci. Technol. **29**(12), 120101 (2018).

[6] G. N. Peggs, P. G. Maropoulos, E. B. Hughes, A. B. Forbes, S. Robson, M. Ziebart, and B. Muralikrishnan, "Recent developments in large-scale dimensional metrology," J. Eng. Manuf. **223**(6), 571–595 (2009).

[7] See https://apimetrology.com/wp-content/uploads/2018/09/2018-API-Radian-3D-Laser-Tracker-Systems-Brochure.pdf for API Radian Pro, 2019.

[8] B. Muralikrishnan, D. Sawyer, C. Blackburn, S. Phillips, B. Borchardt, and W. T. Estler, "ASME B89.4.19 performance evaluation tests and geometric misalignments in laser trackers," J. Res. Natl. Inst. Stand. Technol. **114**(1), 21–35 (2009).

[9] S. Aguado, J. Santolaria, D. Samper, and J. J. Aguila, "Influence of measurement noise and laser arrangement on measurement uncertainty of laser tracker multilateration in machine tool volumetric verification," Precis. Eng. **37**, 929–943 (2013).

[10] D. Zhang, S. Rolt, and P. G. Maropoulos, "Modelling and optimization of novel laser multilateration schemes for high-precision applications," Meas. Sci. Technol. **16**(12), 2541–2547 (2005).

[11] H. Chen, Z. Tan, Z. Shi, H. Song, and H. Yan, "Optimization method for solution model of laser tracker multilateration measurement," Meas. Sci. Rev. **16**(4), 205–210 (2016).

[12] H. Zhuang, B. Li, Z. S. Roth, and X. Xie, "Self-calibration and mirror center offset elimination of a multi-beam laser tracking system," Rob. Auton. Syst. **9**, 255–269 (1992).

[13] L. Wang, T.-K. Hon, J. D. Reiss, and A. Cavallaro, "Self-localization of ad-hoc arrays using time difference of arrivals," IEEE Trans. Signal Process. **64**(4), 1018–1033 (2016).

[14] See https://www.etalon-gmbh.com/en/products/lasertracer/ for Etalon GmbH Website, 2019.

[15] J. Dale, B. Hughes, A. Lancaster, A. Lewis, A. Reichold, and M. Warden, "Multi-channel absolute distance measurement system with sub ppm-accuracy and 20 m range using frequency scanning interferometry and gas absorption cells," Opt. Express, **22**(20), 24869–24893 (2014).

[16] R. Mautz, "Indoor positioning technologies," Habilitation thesis, ETH Zurich, 2012.

[17] R. Schmitt, S. Nisch, A. Schönberg, F. Demeester, and S. Renders, "Performance evaluation of iGPS for industrial applications," in Proceedings of the International Conference on Indoor Positioning and Indoor Navigation (IPIN), Zurich, Switzerland, 2010.

[18] J. E. Muelaner, Z. Wang, O. Martin, J. Jamshidi, and P. G. Maropoulos, "Verification of the indoor GPS system, by comparison with calibrated coordinates and by angular reference," J. Intell. Manuf. **23**(6), 2323–2331 (2012).

[19] See https://www.geodetic.com/wp-content/uploads/2019/07/GSI_INCA4_Brochure_2019_print.pdf for Geodetic Systems, Inca 4 - Picture Perfect Measurements - Product Data Sheet, 2019.

[20] J. Guillory, M. Teyssendier de la Serve, D. Truong, C. Alexandre, and J.-P. Wallerand, "Uncertainty assessment of optical distance measurements at micrometer level accuracy for long-range applications," IEEE Trans. Instrum. Meas. **68**(6), 2260–2267 (2019).

[21] D. Stone and J. Ellis, Calibration and Linear Regression Analysis: A Self-Guided Tutorial, available on https://sites.chem.utoronto.ca/chemistry/coursenotes/analsci/LinRegr2b.pdf.

[22] G. Bönsch and E. Potulski, "Measurement of the refractive index of air and comparison with modified Edlén's formulae," Metrologia **35**(2), 133–139 (1998).

© Author(s) 2020